



## Short communication

## Rapid prototyping for neuroscience and neural engineering

Peter Tek<sup>a</sup>, Terry C. Chiganos<sup>a</sup>, Javeed Shaikh Mohammed<sup>a</sup>, David T. Eddington<sup>a</sup>,  
Christopher P. Fall<sup>a,b</sup>, Peter Ifft<sup>a</sup>, Patrick J. Rousche<sup>a,\*</sup>

<sup>a</sup> UIC Department of Bioengineering, 851 S. Morgan Street, Room 218, Chicago, IL 60607, United States

<sup>b</sup> UIC Medical Center Department of Anatomy and Cell Biology, 808 S. Wood Street,  
Room 578, Chicago, IL 60607, United States

## ARTICLE INFO

## Article history:

Received 30 November 2007

Received in revised form 3 March 2008

Accepted 7 March 2008

## Keywords:

Rapid prototyping

Neuroscience

Neural engineering

Fused deposition modeling

Fabrication

## ABSTRACT

Rapid prototyping (RP) is a useful method for designing and fabricating a wide variety of devices used for neuroscience research. The present study confirms the utility of using fused deposition modeling, a specific form of RP, to produce three devices commonly used for basic science experimentation. The accuracy and precision of the RP method varies according to the type and quality of the printer as well as the thermoplastic substrate. The printer was capable of creating device channels with a minimum diameter of 0.4 or 0.6 mm depending on the orientation of fabrication. RP enabled the computer-aided design and fabrication of three custom devices including a cortical recording/stroke induction platform capable of monitoring electrophysiological function during ischemic challenge. In addition to the recording platform, two perfusion chambers and a cranial window device were replicated with sub-millimeter precision. The ability to repeatedly modify the design of each device with minimal effort and low turn-around time is helpful for oft-unpredictable experimental conditions. Results obtained from validation studies using both the cortical recording platform and perfusion chamber did not vary from previous results using traditional hand-fabricated or commercially available devices. Combined with computer-aided design, rapid prototyping is an excellent alternative for developing and fabricating custom devices for neuroscience research.

© 2008 Published by Elsevier B.V.

## 1. Introduction

With the advent of rapid prototyping (RP), printing technology has become an increasingly useful tool for many engineering applications. The first RP technique originally commercialized in the 1980s revolutionized fabrication techniques by creating solid objects from computer-generated 3D surface models. Automated fabrication eliminated the need for numerically controlled programming and mechanical jigs, thus improving device consistency (Pham and Gault, 1998). Several variations of the original RP technology have evolved including fused deposition modeling (FDM), laminated object manufacturing, electron beam melting and selective laser sintering. Although the resolution, materials, and fabrication techniques remain unique to each RP method, all provide engineers an economical and time-efficient method of rendering, modifying, and fabricating 3D devices (Chua, 1994; Pham and Gault, 1998). As RP technology continues to advance, new applications beyond the classical engineering disciplines are being investigated.

For example, RP is now used to create a wide variety of tissue engineering scaffolds for exogenous tissue growth (Lam et al., 2002; Seitz et al., 2005; Yeong et al., 2004). Researchers hope to eliminate previous problems associated with conventional scaffolding techniques such as inadequate formation of pore networks and imprecise overall morphology by using fused deposition modeling to fabricate the scaffold (Zein et al., 2002). The ability to create artificial vascular networks within the tissue parenchyma would undoubtedly improve interior cell survival and function. In another application, selective laser sintering is used in conjunction with X-ray and/or MRI to create *in vivo* models of patient anatomy. Such 3D models allow physicians to better appreciate the spatial arrangement of anatomical structures and disease entities (McGurk et al., 1997; Potamianos et al., 1998).

Given the large amount of custom machining inherent in typical neuroscience/neural engineering applications, RP may prove broadly applicable to this field as well. Neural engineers often create new devices to overcome minor problems commonly associated with the use of biosensors. The complexities of targeting specific anatomical locations and the stability of the device/tissue interface after insertion are often overlooked. Such inconsistency may be a significant source of experimental error and/or performance limitations. Currently, neuroscience researchers tend

\* Corresponding author. Tel.: +1 312 996 2333; fax: +1 312 996 9465.

to rely on long-established techniques that do not exploit technological progress. For example, dental acrylic is often used to secure electrodes, cannulas and other devices to the skull following implantation into the central nervous system (Crouzier et al., 2006; Miyata et al., 1999). Although simple solutions often suffice, advanced applications such as perfusion chambers and cranial windows require precise and complex structures (Fujita et al., 2000). Additionally, manual fabrication of complex devices often exhausts precious physical resources as well as unnecessary man-hours. RP eliminates the need for specialized fabrication tools and machine shops, and allows for repeated design modification at minimal cost following the initial machine investment.

RP fabrication offers additional benefits beyond ease of design and fabrication. For example, the use of computational design gives the researcher precise control of internal structures that is not attainable with conventional manufacturing techniques such as milling. Furthermore, computer-aided design enables computational modeling and finite element analysis prior to fabrication. Fluid flow analysis or heat/stress distribution profiles can be obtained from computational models, thus allowing for re-design and device optimization with minimal effort.

The present study introduces rapid prototyping technology as a tool to create devices frequently required for neuroscience research. The original purpose of exploring RP technology for neuroscience applications came from the specific need for a skull-based housing platform for stroke electrophysiology research. Due to the relative ease of fabrication and successful *in vivo* implementation of the stroke platform, the use of RP was expanded to other commonly used devices in neural engineering research such as cranial windows and perfusion chambers. Although current FDM-based technology does not permit micron-scale design, thermoplastic devices of millimeter resolution can be easily created and modified with excellent reproducibility. To demonstrate the utility of RP for neuroscience applications, a cranial window, two imaging compatible perfusion chambers and a custom cortical recording platform were rendered and fabricated.

## 2. Material and methods

### 2.1. Device design

Each device was designed using basic geometric modeling software (AutoCad 2007, Autodesk Inc., SAN RAFAEL, CA) and converted to stereolithography (STL) file format. The STL designs were subsequently transferred to a 3D printer (Stratasys Inc., EDEN PRAIRIE, MN) controlled by device-specific interface software. The printer uses the fused deposition modeling method of rapid prototyping to fabricate each structure. Specifically, a computer-controlled nozzle deposits a heated thermoplastic resin within the *x–y* plane according to the device design. The 3D structure is built by sequentially stacking new layers to the existing structure along the *z*-axis. The printer permits a maximum device size of 203 mm × 203 mm × 305 mm with minimum thickness resolution of 0.178 mm. All devices were created using acrylonitrile butadiene styrene (ABS). ABS is a standard thermoplastic material used for RP fabrication due to its durability, strength and rapid liquid–solid phase transition. Following fabrication, the devices were placed in an ultrasonic cleaner filled with 30% NaOH solution to dissolve the base support material.

### 2.2. Accuracy and precision

The accuracy and precision of the FDM printer was quantified by rendering and fabricating multiple rectangular blocks with cylin-

drical channels of progressively smaller diameter. Each rectangular block ( $n = 10$ ) contained 10 cylindrical channels, ranging in diameter from 0.1 to 1.0 mm. Five of the test blocks contained channels printed along the *z*-axis, and the remaining five blocks contained channels printed along the *x–y* plane. The actual diameter of each hole was determined by averaging three individual measurements obtained using a digital caliper under a microscope. For smaller diameter measurements the caliper tip was placed along the base edge of the channel under a microscope to ensure accuracy. By printing the cylindrical channels along both the *z* and *x–y* directions individually, the accuracy and precision data can be combined to assess the 3D resolution of the FDM printer.

### 2.3. Animal experiments

To determine the *in vivo* efficacy of the stroke platform, the device was affixed to the skull of a male, Sprague–Dawley rat (400 g) and used to obtain electrophysiological recordings during stroke. The acute surgery was conducted in compliance with the AAALAC-accredited Animal Care Committee of the University of Illinois at Chicago. Anesthesia was induced using a 4.0% halothane mixture for 10 min followed by an intramuscular injection of KXA (0.1 ml/100 g body weight mixture of Ketamine, 100 mg kg<sup>-1</sup>, Xylazine, 5 mg kg<sup>-1</sup>, Acepromazine, 2.5 mg kg<sup>-1</sup>). Supplemental 0.1 ml doses of KXA were injected throughout the experiment to maintain adequate anesthesia. Pulse rate, oxygen saturation levels and the paw-pinch reflex were used to assess the depth of anesthesia during surgery. Briefly, a 2-cm midline incision was made on top of the head and the subcutaneous tissues were separated and/or incised to gain access to the skull surface. A 5 mm × 5 mm craniectomy was made using 5-mm diameter hand-operated trephine bit to expose the dura. The center of the craniectomy site was located 5.0 mm posterior and 5.5 mm lateral to bregma. Prior to fixation of the device, the dura was delicately removed without causing visible damage to the cortical surface to allow for implantation of the microwire recording array. Using the device as a guide, two additional holes were drilled through the skull anterior and posterior to the central craniectomy for placement of the bone screws. The device was secured to the skull with two bone screws and the linear microwire electrode array was implanted to a sub-pial depth of 1.0 mm using a manual micromanipulator. Direct visualization of the cortical surface during implantation of the array was permitted by windows located on the lateral aspect of the platform.

## 3. Results

### 3.1. Printer resolution

Rectangular blocks with test holes of progressively increasing diameter (0.1–1.0 mm) were fabricated via RP to assess printer resolution. Five blocks contained holes oriented along the *z*-axis and five blocks contained holes oriented along the *x–y* plane to evaluate the effect of orientation on device accuracy and precision (see Fig. 1). As evidenced by the bar graph of in figure B, the accuracy of the printer varied according to the orientation of fabrication. Test holes created along the *z*-axis more closely approximated the rendered diameters compared to holes created along the *x–y* plane. Although the design of each test block called for test holes with diameters ranging from 0.1 to 1.0 mm, the minimum diameter produced by the printer was 0.4 and 0.6 mm for holes fabricated along the *x–y* plane and *z*-axis, respectively. Although the accuracy of the printer is best for *z*-axis fabrication, the resolution is diminished from being able to print 0.4–0.6 mm.

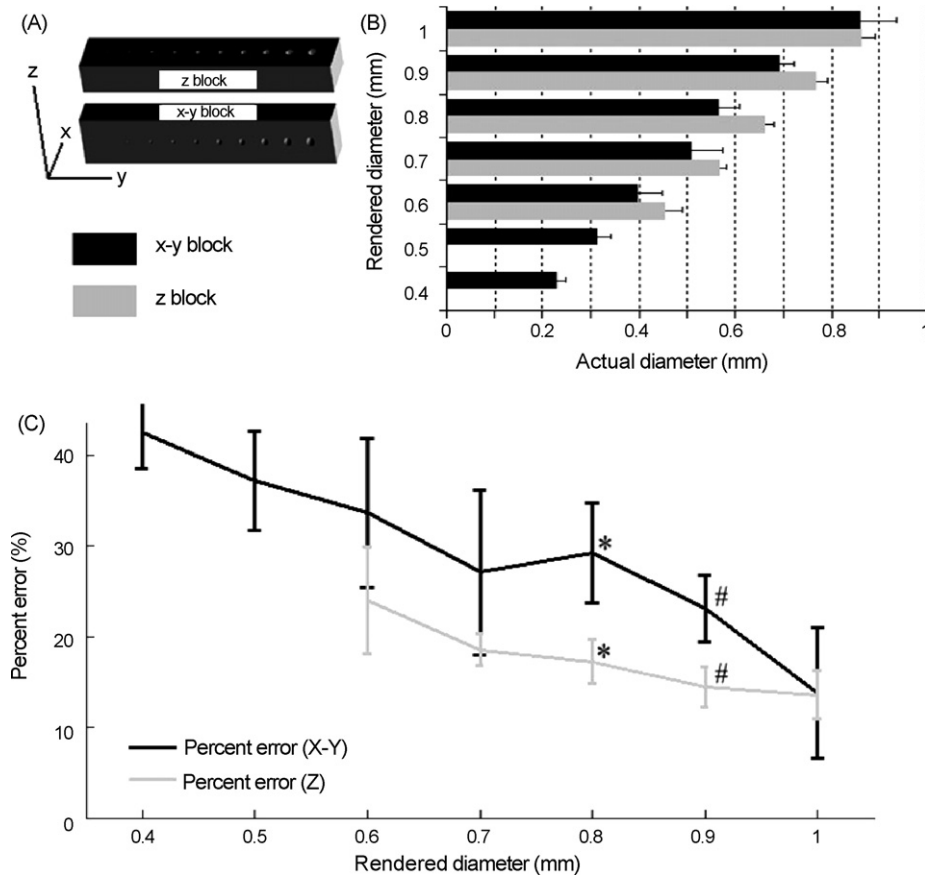


**Fig. 1.** (A) Visual representation of printed bars in  $x$ - $y$  and  $z$  orientations. (B) Bar graph depicting rendered hole diameters relative to the actual measured diameters for test blocks contained cylindrical holes oriented along the  $z$ -axis (gray,  $n = 5$ ) and  $x$ - $y$  plane (black,  $n = 5$ ). (C) As evidenced by the percent error depicted,  $z$ -axis diameters exhibited greater accuracy for each rendered diameter than  $x$ - $y$  diameters. The mean percent errors were statistically distinct for each dimension only at 0.8 and 0.9 mm diameters (student's  $t$ -test,  $p < 0.05$ ). The precision of the RP printer along both the  $z$  and  $x$ - $y$  axes is determined by the standard deviation (error bars) of the actual diameters.

The accuracy of the printer along both dimensions was determined by calculating the percent error of actual diameters relative to rendered diameters. Regardless of dimension, the percent error decreased as the rendered diameter increased.  $Z$  diameters, however, exhibited greater accuracy at all points. A student's  $t$ -test was applied to both data sets to determine if the calculated accuracy differences were statistically distinct. The mean percent errors are statistically distinct only at rendered diameters of 0.8 and 0.9 mm (see Fig. 1C). To determine the precision of the printer (i.e. consistency of fabrication), the standard deviation of the actual diameters was calculated for all points and plotted as error bars in Fig. 1C. Despite an inferior minimum resolution (0.6 mm versus 0.4 mm),  $z$ -axis fabrication exhibited greater accuracy and precision at all tested diameters.

### 3.2. Perfusion chamber

Two distinct perfusion chambers were created to house individual brain slices for *ex vivo* study. The first perfusion chamber represents a prototype device that is combined with an array of microfluidic channels (see Fig. 2) to tightly regulate flow parameters within the tissue bath. The microfluidic channels address the flow of neurochemicals and other fluids to precise locations in the brain slice with a temporal profile that is controlled by the user. Due to the repeated design modifications necessary when developing a new system, the use of commercially available flow chambers becomes cost-prohibitive. RP allows for cost-effective iteration of the chamber configurations to accommodate a var-

ied range of experimental conditions, as well as the fabrication of novel perfusion chambers with relative ease. In addition, RP allows researchers to analyze fluid flow characteristics with computational modeling, thus providing information to help optimize experimental designs highly dependent on temporal properties. The chamber allows for perfusion of large tissue slices and provides access for patch clamp recording, intracellular/extracellular recording or imaging studies.

The behavior of the perfusing ACSF in the new chamber was visually inspected and found to be similar to commercially available chambers. The perfusing ACSF was connected to standard connectors and a peristaltic pump was used to perfuse the chamber. The stimulus was injected through the microfluidic channels via passive pumping, which does not require external pumps or tubing (Walker and Beebe, 2002). Briefly, differences in surface tension at the inlet and outlet ports drive fluid through the microchannels. As passive pumping operates with extremely low pressures, the slice was not deflected over the vias. The device was validated using fluorescent dye delivered to the slice. The intensity of the injected dye was monitored as a function of time. As the chamber design is identical to commercially available systems, we expect a similar slice viability time of 4–8 h.

The second type of perfusion chamber simultaneously houses multiple brain slices for NMR analysis. Previous investigators have created a custom perfusion chamber to allow for simultaneous study of multiple excised brain slices using nuclear magnetic resonance imaging (NMR). According to Shepherd et al. (2002), the perfusion chamber consisted of six rings lathed to fit within a

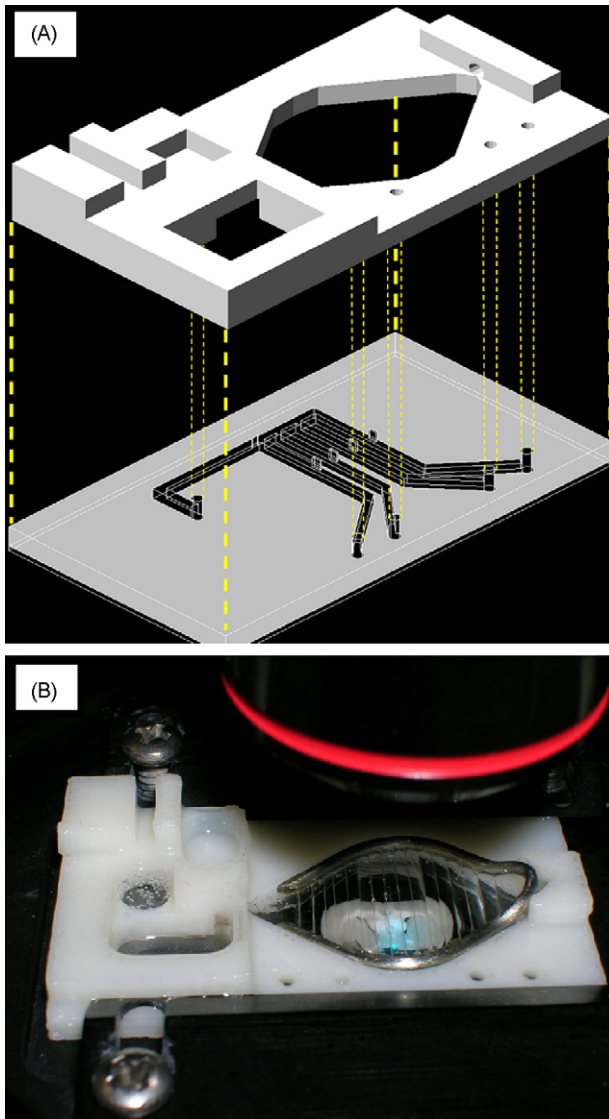


**Fig. 2.** (A) CAD rendering of the standard perfusion chamber prepared via RP married with microfluidic channels. (B) Image of a brain slice in the custom perfusion chamber fabricated with the 3D printer.

15-mm diameter NMR tube (Shepherd et al., 2002). The bottom ring of the tube contained a port for unhindered flow of perfusate. Polyvinylchloride tubing was attached via epoxy resin to the first ring, and additional rings (each containing a coronal brain slice) were stacked to construct the perfusion tube.

To replicate the perfusion chamber using RP, the rings and vertical support piece were designed and fabricated separately before assembly and insertion into the NMR tube. To avoid the logistical complications of attaching tubing to each ring, an inflow channel was fabricated directly within the bottom ring and each ring spacer contained a groove to fit along the inflow channel (see Fig. 3). Nylon mesh was attached to the underside of each spacer to support the brain slices.

### 3.3. Cranial window

Levasseur et al. (1975) first described a method for creating a simple pressurized cranial window. Consisting only of a circular glass cover slip and a stainless steel ring, the original device allowed researchers to view the cortical vasculature while main-

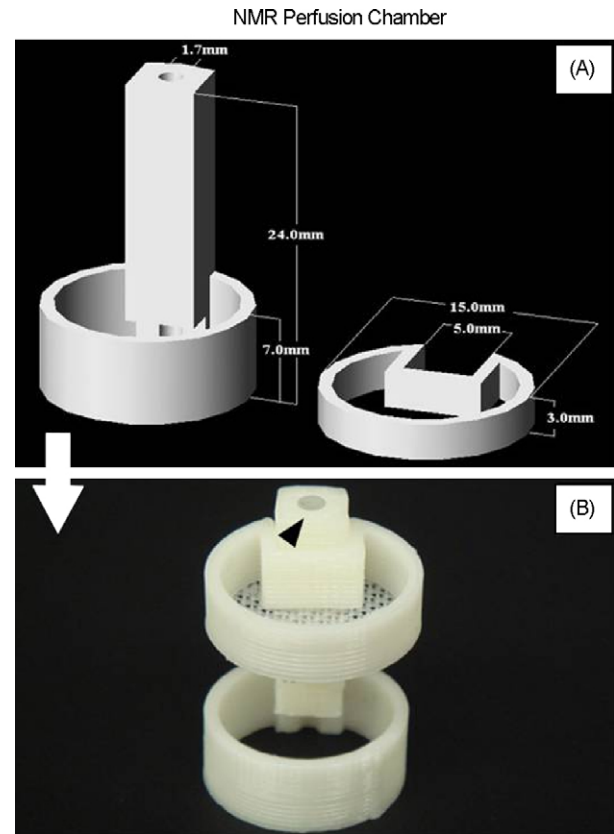


**Fig. 3.** (A and B) 3D CAD rendering and photograph of the NMR perfusion chamber. Multiple rings (depicted at right of panel A) each housing one brain slice can be stacked and attached to the vertical support. The support contains one channel oriented along the vertical axis of the device (see arrow, panel B) for inflow of perfusate. The entire device is placed into an NMR tube and inserted into the magnet for analysis.

taining intracortical pressure during acute experimentation. Due to the lack of readily available pressurized cranial windows, repeated custom manufacturing of the device often becomes time consuming. RP allows for the creation of cranial windows with relatively low-turn-around time. Devices can also be fabricated to precisely fit each particular animal experiment with relative ease, thus providing highly specific devices to match the varied nature of individual animals.

The cranial window fabricated by RP consisted of three pieces; a circular plastic cover slip, a base, and top. The transparent cover slip is placed on top of the base to seal the chamber yet permit external viewing of the cortical surface. The device contains five channels in total located around the periphery of the window. Two small channels permit flushing of the cortical surface, one channel is used to regulate surface pressure, and the final two serve as bone screw channels to anchor the device to the skull (see Fig. 4).

### 3.4. Cortical recording platform

The original FDM-fabricated device was intended to house a linear array of microwire cortical electrodes for assessment of electrophysiological function during stroke in a rat model. The complexity involved in accurately placing multiple biosensors into cortical tissue and maintaining a stable recording environment necessitates the use of a housing platform. Prior to using RP, hand-made devices created with dental acrylic were often difficult to set up and recreate. RP allows for more precise and reproducible fabrication of recording platforms, thus improving the accurate

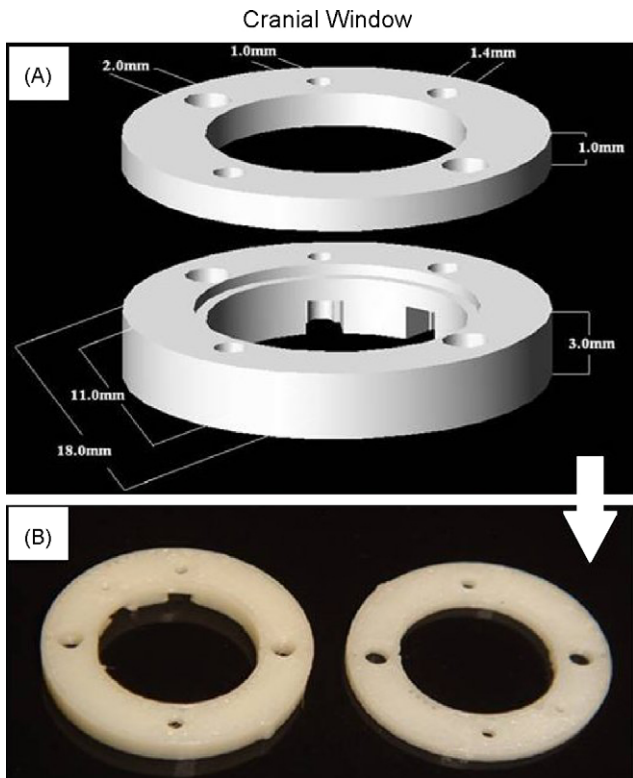


**Fig. 4.** (A and B) 3D CAD rendering and photograph of the cranial window device. A circular plastic cover is placed between the components of the device prior to fixation to the skull. Each ring contains five holes: two for bone screws (2.0 mm diameter), two for inflow/outflow of perfusate (1.4 mm diameter) and a final channel for pressure regulation (1.0 mm diameter).

placement of the biosensors. In addition, the platform provides a rigid and stable setup throughout experimental conditions.

The artificially induced stroke is created by intravenous injection of rose bengal dye and simultaneous illumination of a specific region of the cortex via a micro-fiber optic light probe. Upon adequate light exposure, highly reactive oxygen radicals are created initiating platelet aggregation. The artificial method of microvascular occlusion causes tissue damage consistent with naturally occurring ischemic infarcts. Additionally, the resultant cortical lesion is limited to the region of cortex that received adequate illumination, thus allowing for precise control of lesion location and morphology (Chiganos et al., 2006). RP was used to create a monolithic skull-based platform to house both the linear array of electrodes and the fiber optic light probe for stroke induction, thus precisely fixing the location of the recording electrodes relative to the lesion (see Fig. 5). The highlighted rectangular area (6 mm × 1.5 mm) is used to hold the electrode array, and a cylindrical channel (2 mm diameter) located anterior to the electrode chamber permits passage of the fiber optic light probe directly to the pial surface for stroke induction. Additionally, 4 mm × 2 mm open windows located on each side of the device allowed for direct visualization of the cortical surface during insertion of the electrode wires and stroke induction. The platform was secured to the skull surface using two bone screws located along the long axis of the device.

A single, acute animal experiment was performed to validate the *in vivo* efficacy of the stroke induction/microwire recording platform. Although initially the device was difficult to attach due to the natural curvature of the skull, the designated channels for the light probe and microwire electrodes proved extremely useful for fixing the relative positions of the resulting lesion and recording sites. Fol-

lowing the craniectomy and drilling of bone screw holes, the device was secured to the skull and the electrode array was implanted into the cortical gray matter under direct visualization. After implantation, the micromanipulator was removed from the electrode and used to independently lower the fiber optic probe to the cortical surface. The platform eliminated the need for two micromanipulator arms by securing the electrode after implantation. The use of two arms to independently control the light probe and electrode is cumbersome and logistically difficult due to the relatively small operating field. Fig. 5C shows the attachment of the device to the skull and figure B displays the firing rate change for a single perinfarct neuron cluster recorded before, during and after stroke. As expected, the firing rate initially increases after stroke initiation before progressively decreasing to sub-normal levels 40 min after stroke (Chiganos et al., 2006). The firing rate is expected to decrease as electrophysiological function is compromised due to prolonged and irreversible ischemia.

#### 4. Discussion

The use of RP technology for basic neuroscience research will alleviate many common issues associated with manual fabrication of complex, commercially unavailable devices. Computerized design allows researchers to perform computational modeling such as fluid flow and stress/strain analyses prior to fabrication of the device, eliminating the need for repeated empirical testing and multiple prototypes. Compared to hand or custom machine fabrication, computerized manufacture can drastically reduce device manufacturing time and errors while increasing device performance reliability, consistency and repeatability. In the stroke application, use of RP saved roughly 6 h of electrode manufacture and set-up time while (more importantly) increasing the accuracy of our electrode placement. The present report demonstrates the ability to design, render and build a variety of devices with relative ease and excellent reproducibility.

All devices were fabricated with minimal complications using the 3D printer made by Stratasys Inc. Some distortion of the bone screw channels occurred infrequently during fabrication of the stroke/recording platform, and additional extraneous drops of thermoplastic resin were observed near the upper surface of several devices. Overall, less than 10% of all devices had a directly observable flaw (e.g. extra resin or channel distortion) rendering less than 5% unusable for experimentation. Occasional leaks were noted for the perfusion chamber and cranial window that were easily sealed with wax. Overall the printer demonstrated excellent reproducibility with an acceptably low error rate.

Although the cortical recording platform provided a simple way to monitor the electrical activity of neurons after infarction of adjacent cortex, the device proved difficult to secure to the rat cranium. The length of the device relative to the anterior–posterior dimension of the rat cranium precludes the precise positioning of the platform for analysis of specific functional cortices. The platform, however, fixed the relative location of the microwire electrodes to the lesion rim, thus allowing for a more quantifiable and controlled assessment of neural activity as a function of exact distance from the infarct. Recordings made with the RP platform were otherwise identical to those obtained from standard hand-manufactured electrodes (Chiganos et al., 2006). Small imperfections of the perfusion chamber also caused minor difficulties during experimental use. Missing facets and additional resin caused occasional leakage of saline from the enclosed chamber. Despite the minor complications, optical imaging obtained after the devices were sealed showed no variation from studies obtained from commercially available chambers (Shaikh Mohammed et al., 2007).

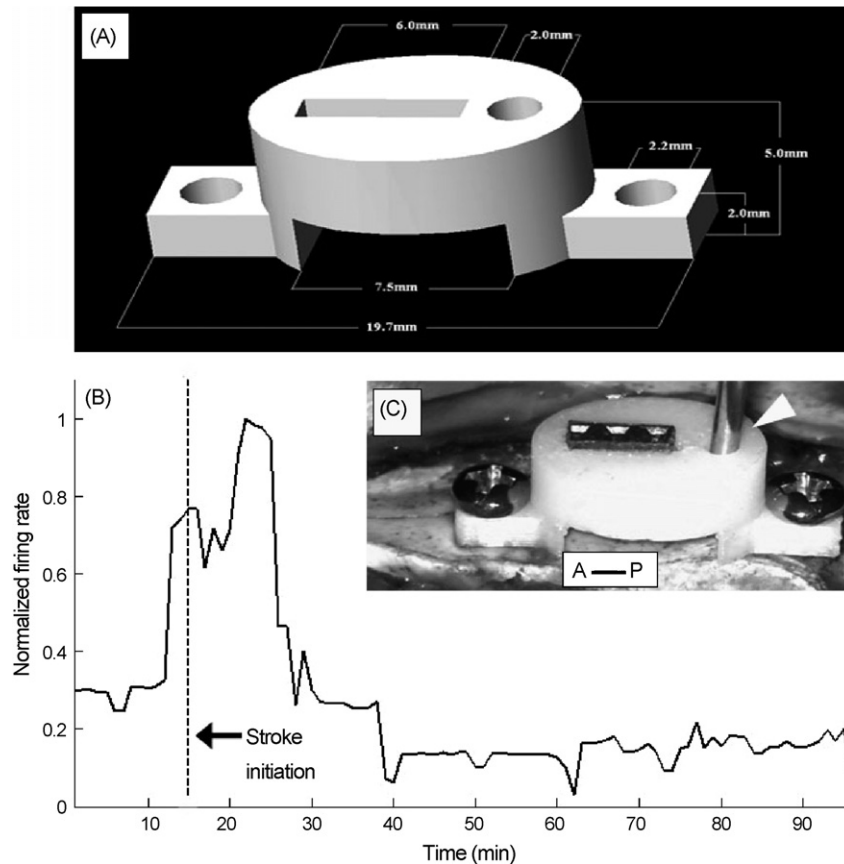


**Fig. 5.** (A) CAD rendering of the stroke platform, containing a 6.0mm rectangular port for insertion of the microwire recording array and 2.0-mm diameter guide port for insertion of the fiber optic probe. (B) Sample data obtained using the stroke platform. The normalized firing data from a neuron cluster next to the phot thrombosis-mediated stroke exhibits a marked decrease after illumination of the cortex and intravenous injection of rose bengal. (C) Actual device affixed to the parietal bone with fiber optic probe (white carrot) and 3-channel microwire array (not connected). Anterior–posterior axis indicated by figure inset (A–P).

Attempts to create smaller designs using the RP process produced devices with distortions and fused features. Such deviation of the actual device from the rendered geometric model is the direct consequence of the limited minimum spatial resolution of the printer. Specifically, the resolution is governed by the printer's ability to melt small volumes of ABS polymer. The resolution along each orthogonal axis is largely governed by the quality of the nozzle used to extrude the polymer. While other materials such as  $\epsilon$ -caprolactone may be a viable alternative to help improve resolution, ABS remains an ideal substrate for neuroscience applications due to its durability and biocompatibility (Ahn et al., 2002; Zein et al., 2002). Furthermore, ABS is resistant to mild fluctuations of temperature or humidity, and unaffected by aqueous acidic environments (Harper, 2002).

The resolution limitations described by the present study are specific to the particular model of FDM printer used to fabricate the devices. The limitations are not inherent to rapid prototyping and prove less significant as the size of the animal subject increases. Other commercially available methods of RP such as 3D printing report resolutions approaching the 100  $\mu\text{m}$  range while new emerging methods like microstereolithography near 5  $\mu\text{m}$  resolution (Bertsch et al., 1997). Resolution is also lost during conversion from CAD renderings to STL format. Standard STL conversion results in a triangular, semi-regular tessellation of the original CAD design.

Regardless of the limitations imposed by the printer, RP proved highly useful in creating a wide variety of devices. Beyond the original stroke induction/microwire recording platform, the perfusion chamber designed for use in a vertical bore magnet allows

researchers to use high field NMR to study explanted brain slices. The inflow channels were built directly into the system to avoid complex tubing systems and to prevent accidental kinks. Without the use of expensive machining, a cranial window device was successfully replicated for unhindered viewing of the cerebral vasculature. The devices presented herein only represent a small sampling of the potential for RP in neuroscience/neural engineering research. As printer technology continues to improve, RP should be considered as a cost-effective and highly adaptable method of fabrication for specialized, complex research components.

#### Acknowledgements

The authors want to thank Amani Abuhabsah at the UIC Department of Bioengineering for technical assistance. The project was funded by the NSF CAREER AWARD (grant no BES00348145) for PJR, NIH (grant no. MH-64611) and the NARSAD Young Investigator Award for CPF.

#### References

- Ahn SH, Montero M, Odell D, Roundy S, Wright PK. Anisotropic material properties of fused deposition modeling ABS. *Rapid Prototyping J* 2002;8(4):248–57.
- Bertsch A, Yezequel JY, Andre JC. Study of the spatial resolution of a new 3D microfabrication process: the microstereolithography using a dynamic mask-generator technique. *J Photochem Photobiol A: Chem* 1997;107(July (1–3)):275–81.
- Chiganos Jr TC, Jensen W, Rousche PJ. Electrophysiological response dynamics during focal cortical infarction. *J Neural Eng* 2006;3(December (4)):L15–22.

- Chua CK. 3-Dimensional rapid prototyping technologies and key development areas. *Comput Control Eng J* 1994;5(August (4)):200–6.
- Crouzier D, Baubichon D, Bourbon F, Testylier G. Acetylcholine release, EEG spectral analysis, sleep staging and body temperature studies: a multiparametric approach on freely moving rats. *J Neurosci Methods* 2006;151(March (2)):159–67.
- Fujita H, Matsuura T, Yamada K, Inagaki N, Kanno I. A sealed cranial window system for simultaneous recording of blood flow, and electrical and optical signals in the rat barrel cortex. *J Neurosci Methods* 2000;99(June (1–2)):71–8.
- Harper CA. *Handbook of plastics, elastomers and composites*. New York: McGraw Hill; 2002. pp. 160–167.
- Lam CXF, Mo XM, Teoh SH, Hutmacher DW. Scaffold development using 3D printing with a starch-based polymer. *Mater Sci Eng C: Biomim Supramol Syst* 2002;20(May (1–2)):49–56.
- Levasseur JE, Wei EP, Raper AJ, Kontos AA, Patterson JL. Detailed description of a cranial window technique for acute and chronic experiments. *Stroke* 1975;6(May (3)):308–17.
- McGurk M, Amis AA, Potamianos P, Goodger NM. Rapid prototyping techniques for anatomical modelling in medicine. *Ann R Coll Surg Engl* 1997;79(May (3)):169–74.
- Miyata G, Fetissov SO, Meguid MM. A complication of long-term brain microdialysis. *Nutrition* 1999;15(September (9)):723–4.
- Pham DT, Gault RS. A comparison of rapid prototyping technologies. *Int J Mach Tools Manuf* 1998;38(October (10–11)):1257–87.
- Potamianos P, Amis AA, Forester AJ, McGurk M, Bircher M. Rapid prototyping for orthopaedic surgery. *Proc Inst Mech Eng [H]* 1998;212(5):383–93.
- Seitz H, Rieder W, Irsen S, Leukers B, Tille C. Three-dimensional printing of porous ceramic scaffolds for bone tissue engineering. *J Biomed Mater Res Part B: Appl Biomater* 2005;74B(August (2)):782–8.
- Shaikh Mohammed J, Caicedo H, Fall CP, Eddington DT. Brain slice stimulation using a microfluidic network and standard perfusion chamber. *J Visual Exp* 2007; 8.
- Shepherd TM, Blackband SJ, Wirth III ED. Simultaneous diffusion MRI measurements from multiple perfused rat hippocampal slices. *Magn Reson Med* 2002;48(September (3)):565–9.
- Walker G, Beebe DJ. A passive pumping method for microfluidic devices. *Lab on Chip* 2002;2(3):131.
- Yeong WY, Chua CK, Leong KF, Chandrasekaran M. Rapid prototyping in tissue engineering: challenges and potential. *Trends Biotechnol* 2004;22(December (12)):643–52.
- Zein I, Hutmacher DW, Tan KC, Teoh SH. Fused deposition modeling of novel scaffold architectures for tissue engineering applications. *Biomaterials* 2002;23(February (4)):1169–85.